ЖЭТФ, 2021, том 159, вып. 4, стр. 690–695 © 2021

CRITICAL FLUCTUATIONS BEYOND THE QUANTUM PHASE TRANSITION IN DZYALOSHINSKII–MORIYA HELIMAGNETS $Mn_{1-x}Fe_xSi$

S. V. Grigoriev [a,b*], ***O. I. Utesov*** [a,b], ***N. M. Chubova*** [a], ***C. D. Dewhurst*** [c], ***D. Menzel*** [d], ***S. V. Maleyev*** [a]

[a] *Petersburg Nuclear Physics Institute named by B. P, Konstantinov of National Reserarch Centre "Kurchatov institute" 188300, Saint Petersburg, Gatchina, Russia*

[b] *Saint Petersburg State University 198504, Saint Petersburg, Russia*

[c] *Institut Laue–Langevin 38042, Grenoble, Cedex 9, France*

[d] *Technische Universität Braunscheig 38106, Braunschweig, Germany*

Received December 1, 2020,
revised version December 1, 2020
Accepted for publication December 3, 2020

Contribution for the JETP special issue in honor of I. E. Dzyaloshinskii's 90th birthday

DOI: 10.31857/S0044451021040106

Many years have passed since the first observation of helical spin structures in cubic B20 compounds FeGe [1] and MnSi [2]. However, helimagnets with Dzyaloshinskii–Moriya (DM) interaction [3,4] are among the most studied systems in contemporary condensed matter physics. In particular, this interest is stimulated by rather simple but fancy phase diagram which includes topologically lattice (A-phase) [5]. The theoretical descriptions [6,7] pointed out that the competition between the ferromagnetic exchange interaction and the antisymmetric DM interaction is balanced in the homochiral helical magnetic structure.

Mixed B20 compounds like $Mn_{1-x}Fe_xSi$ or $Mn_{1-x}Fe_xGe$ are characterized by additional parameter x which allows fine tuning for the system properties. In $Mn_{1-x}Fe_xGe$ its variation leads to change of the sign of magnetic chirality at $x_c \approx 0.75$ [8, 9], where the system is in ferromagnetic state due to cubic anisotropy [10].

The isostructural solid solutions $Mn_{1-x}Fe_xSi$ also reveal intriguing properties upon Fe concentration growth. The substitution of manganese by iron suppresses the helical order [11]. Neutron scattering studies [12, 13] together with magnetic susceptibility and specific heat measurements [11, 14–16] discovered a quantum critical point (QCP) described as a suppression of the spiral phase with long-range order (LRO) in $Mn_{1-x}Fe_xSi$. As it was shown in Refs. [13, 15, 16], this QCP located at $x_c \approx 0.11$–0.12 is hidden by an extensive phase of spin helix fluctuations. This fluctuation regime, sometimes referred to as chiral spin liquid [17, 18], vanishes at about $x \approx 0.24$.

Both magnetic susceptibility measurements and neutron scattering experiments demonstrate a short-range order (SRO) and a crossover to the helix fluctuating regime [13, 19–21]. The crossover temperature T_{DM} decreases with x and becomes zero at $x_{DM} \approx 0.17$ [12, 22]. It was shown that the temperature T_{DM} is proportional to the spin wave stiffness of the compounds $Mn_{1-x}Fe_xSi$ [23]. One concludes that these compounds at $x \sim x_{DM} \approx 0.17$ represent the only known example of the system, where ferromagnetic exchange approaches zero but

* E-mail: grigoryev_sv@pnpi.nrcki.ru

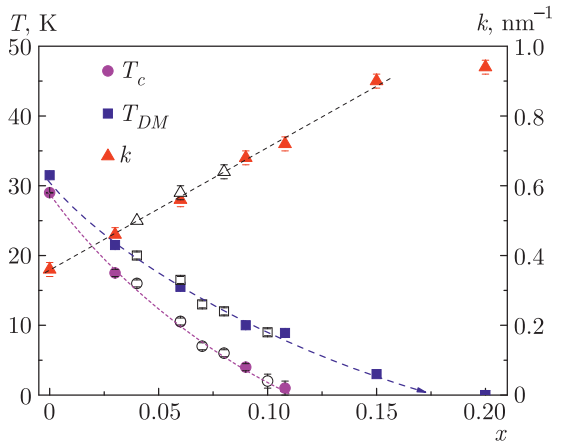

Fig. 1. (Color online) Temperature–concentration (T–x) phase diagram of the $Mn_{1-x}Fe_xSi$ compounds and the helix wave vector k as a function of x. The data taken from several studies [12, 13, 23] are combined with data of the present work. The dashed lines are the guides for an eye

DM interaction is finite and provides chiral rotation of spins in magnetic fluctuations.

In the present paper, we study the critical fluctuations in DM helimagnets $Mn_{1-x}Fe_xSi$ by means of polarized neutron scattering. Three samples with $x = 0.10$, $x = 0.15$, and $x = 0.20$ are selected so as to represent three different regimes: namely close to the quantum critical point $x \sim x_c$, close to the concentration with zero ferromagnetic exchange x_{DM}, and beyond this concentration, respectively.

The series of $Mn_{1-x}Fe_xSi$ single crystals with $x = 0.10$, 0.15, 0.20 were grown using the Czochralski technique at the Institute of Condensed Matter Physics (Braunschweig, Germany). These samples were prepared as cylinders with a height of 15–20 mm and a diameter of 5–6 mm.

The temperature–concentration (T–x) phase diagram is shown in Fig. 1. One can see (in accord with Refs. [13, 15, 16, 19]) that T_c, which indicates a phase with LRO, reaches zero at $x_c \approx 0.11$–0.12, while the temperature band of the fluctuating helix regime increases with x. The decrease in T_c is accompanied by the linear with x increase in the helix wave vector k, as shown in Fig. 1.

The polarized small-angle neutron scattering (SANS) was performed using the D22 instrument at the Laue–Langevin Institute (Grenoble, France). The [110] axis of the single crystal was oriented parallel to the neutron beam with an accuracy of 5°. A polarized neutron beam with initial polarization $P_0 = 0.93$ and mean wavelength $\lambda = 0.60$ nm was used. The scattered neutrons were detected with a 2D position sensitive detector. The beam divergence was tuned from 1 to 10 mrad to set the Q-range and Q-resolution optimal for an individual sample ($\mathbf{Q}$ is a momentum transfer). With these settings, we were able to cover the Q-range from $2 \cdot 10^{-2}$ to 2 nm^{-1}. A weak magnetic field (1 mT) guiding the polarization $\mathbf{P}_0$ was applied along the Q_x. The temperature was set in the range from 1.7 to 60 K with accuracy of the order of 0.05 K. As a result, we obtain the maps of polarized SANS intensities at various temperatures for three samples with different x. A background intensity maps were taken for all samples at high temperature ($T = 60$ K) when no magnetic scattering is observed. These background maps were subtracted from the other scattering maps of the given sample. The software GRASP developed at the ILL (Grenoble) were used for the primary data reduction [24].

Figure 2 shows the maps of the polarized SANS intensities with the polarization along $\mathbf{P}_0$. One can follow the evolution of the scattering patterns with temperature (vertical axis) and the concentration (horizontal axis). The whole diagram can be qualitatively described in the following way. No scattering is observed at the temperature of 15 K for all three concentrations. Upon lowering temperature to 9 K, the blurred but well detectable scattering appears for the sample with $x = 0.10$, while the samples with $x = 0.15$ and $x = 0.20$ show no scattering, demonstrating absence of short-range magnetic correlations. Further temperature lowering to 5 K forms a well-defined "half-moon" image (which is typical for chiral helimagnets) for the sample with $x = 0.10$. For the ones with $x = 0.15$ and $x = 0.20$, it results in the appearance of the blurred images. At $T = 2$ K, the scattering for the sample with $x = 0.10$ is almost the same, whereas for the sample with $x = 0.15$, a slightly blurred half-moon image appears. For the most disordered sample with $x = 0.20$, the image is still far from being well-defined half-moon. We note that the scattering is strongly asymmetric in all cases. The latter is typical for the critical scattering above T_c in the MnSi system [20, 21, 25].

Similarly to Ref. [26], we treated the obtained data using the following mean-field form of the neutron cross section which is appropriate for the disordered fluctuating phase in these compounds ($T > T_c$) [20, 25]:

$$\frac{d\sigma}{d\Omega} = \frac{r^2 T}{A} \frac{k^2 + \kappa^2 + Q^2 + 2\,\mathrm{sgn}\,(D)\, k\mathbf{Q} \cdot \mathbf{P}_0}{\left[(Q+k)^2 + \kappa^2\right]\left[(Q-k)^2 + \kappa^2\right]}. \quad (1)$$

Here $\mathbf{Q}$ is the scattering vector, r is the classical electron radius, κ is the inverse correlation length of the

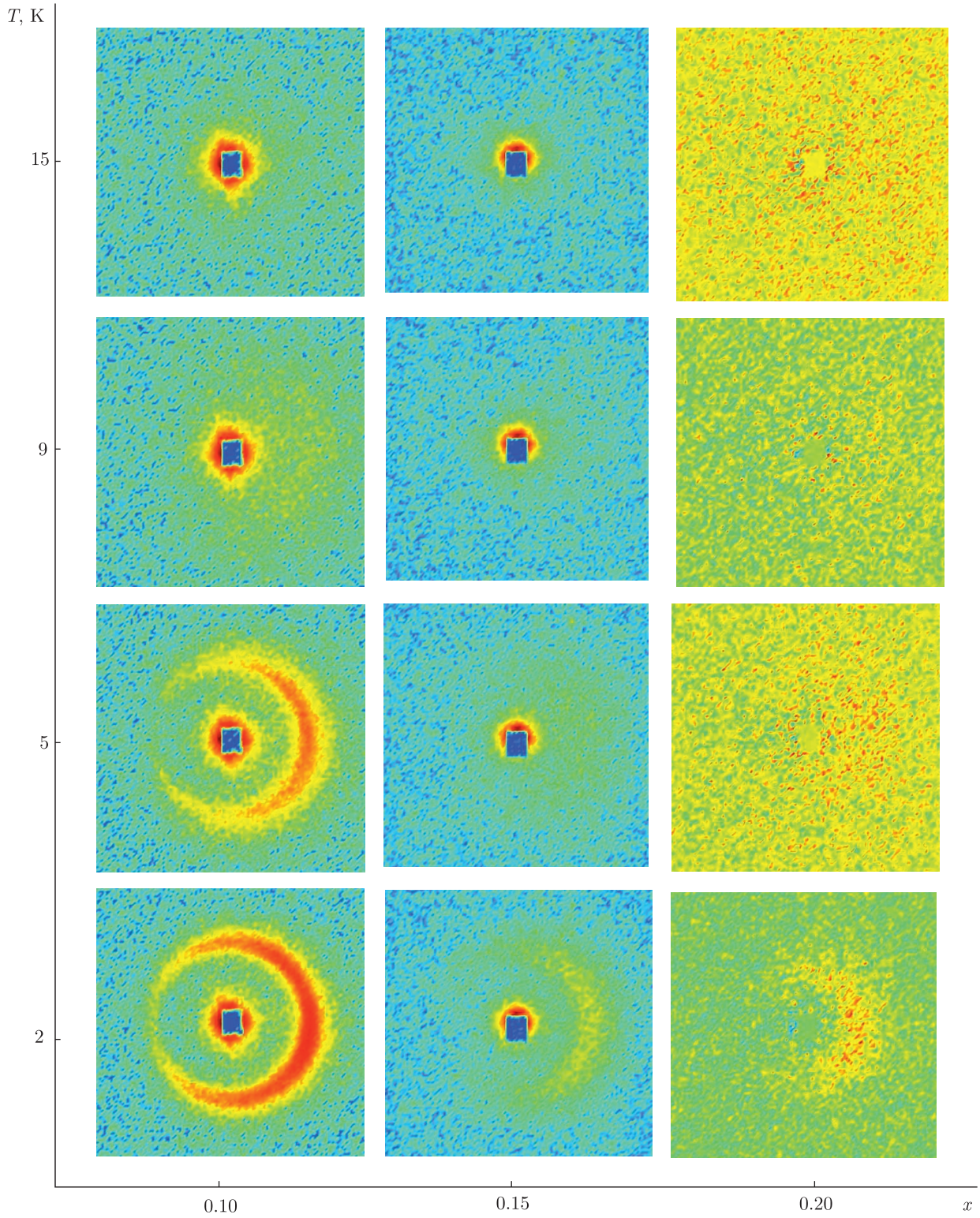

Fig. 2. (Color online) Maps of the polarized SANS intensities plotted on the T–x phase diagram for $Mn_{1-x}Fe_xSi$ system for the polarization $\mathbf{P}_0$ along the guide field

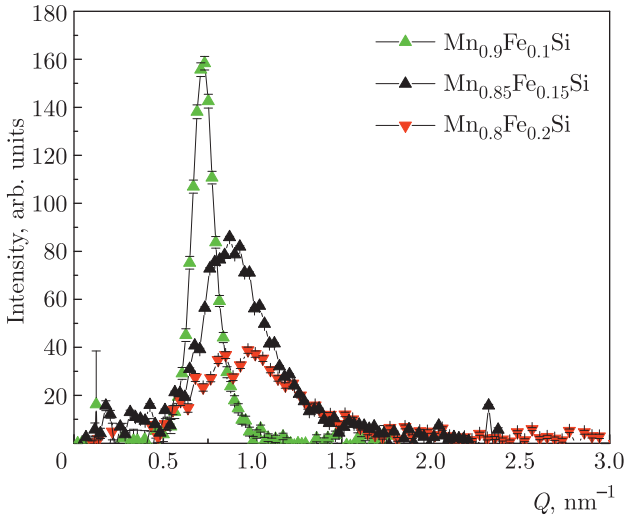

Fig. 3. (Color online) Q-dependence of the azimuthally averaged scattering intensity for the $Mn_{1-x}Fe_xSi$ system with $x = 0.10, 0.15, 0.20$ at $T = 2.0$ K

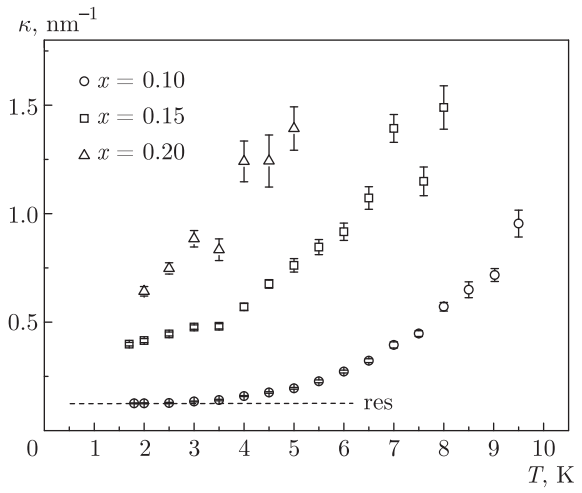

Fig. 4. Temperature dependence of the inverse correlation length of helical fluctuations for the $Mn_{1-x}Fe_xSi$ system with $x = 0.10, 0.15, 0.20$ in the log-log scale (the line denoted "res" shows the level of the instrumantal resolution)

critical fluctuation, A is the spin wave stiffness at low temperatures, D is the Dzyaloshinskii constant, and $\mathbf{P}_0$ is the incident polarization of neutrons. The cross section (Eq. (1)) has several features provided by DM interaction.

(i) Due to the second term of the product in the denominator, the scattering intensity should form a sphere of radius $Q = k$ with a width of κ. The scalar variables in $(Q - k)^2$ are due to isotropic DM interaction.

(ii) The intensity has the Lorentzian shape typical for critical fluctuations.

(iii) The scattering intensity is strongly oriented along the incident neutron polarization since the numerator of Eq. (1) is maximal at $\mathbf{P}_0$ parallel to $\mathbf{Q}$ and it is minimal at $\mathbf{P}_0$ antiparallel to $\mathbf{Q}$.

The chirality of the critical fluctuations can be estimated via measurement of the polarization of the scattering:

$$P_s(Q) = \frac{\sigma(\mathbf{P}_0) - \sigma(-\mathbf{P}_0)}{\sigma(\mathbf{P}_0) + \sigma(-\mathbf{P}_0)} = -\frac{2kQP_0\cos\phi}{Q^2 + k^2 + \kappa^2}, \quad (2)$$

where ϕ is the angle between $\mathbf{P}_0$ and $\mathbf{Q}$, and we use Eq. (1) to express its value via parameters Q, k and κ.

For quantitative analysis, the intensity maps were azimuthally averaged. Examples of the radial profiles (the Q-dependence of the scattering intensity) are shown in Fig. 3. As it is well seen in Fig. 3, the position and the width of the observed peak differ for the three samples. The scattering curve $I(Q)$ can be well described by the Lorentzian at high temperatures, which can be ascribed to the scattering on the critical fluctuations of the helical structure, whereas at low temperatures, $I(Q)$ is described by the sum of the Gaussian and Lorentzian for the samples with $x = 0.10$ and $x = 0.15$; Gaussian term being attributed to the limitation of the instrument resolution, which exceeds the value of 0.12 nm^{-1} (see Fig. 3, curve for $x = 0.10$).

The whole set of the experimental data obtained by polarized SANS was fitted to Eq. (1). The position of the maximum k (the helix wavevector) and inverse correlation length κ of the helix were obtained as a result of the fit. The wave vector does not change with the temperature within the error bars for the individual sample. It is equal to 0.72 nm^{-1}, 0.90 nm^{-1}, and 0.94 nm^{-1} for the samples with $x = 0.10$, 0.15, and 0.20, respectively. Interesting to note that the wave vector changes linearly with the concentration in the range of $x = 0$–0.15 and saturates at the concentration x larger that 0.15 (see Fig. 1). It is correlated to the range with the finite crossover temperature T_{DM} in the $Mn_{1-x}Fe_xSi$ compounds.

The temperature dependence of the inverse correlation length κ is shown in Fig. 4. As it was noticed above, the value of κ is resolution limited for the compound with $x = 0.10$ for the low temperature range. It saturates with lowering temperature at $T_c = 3.0$ K ($x = 0.10$). In contrast, for the sample with $x = 0.15$, κ tends to saturate at larger value, disorder-induced κ_d (see below). For the sample with $x = 0.20$, κ does not saturate at all.

We observe (it was also noted in Refs. [20,25]) that the polarization P_s ($Q = k$) is close to 1 at low temperature even for the most disordered sample with $x = 0.20$, which shows that DM interaction is still present and makes short fluctuations chiral. Upon increase of temperature, the polarization P_s was found to decrease smoothly.

The behaviour observed experimentally can be qualitatively understood using the assumption that Fe ions introduce the defect antiferromagnetic (AF) bonds in the system. First of all, strong AF bonds lead to significant lowering of the spin wave stiffness, T_c, and T_{DM}. The latter becomes zero at $x = x_{DM}$. Moreover, according to the theory of Ref. [27], strong AF bonds can lead to large variation of the helical vector even at small concentrations (see Fig. 1).

It is well-known that the strong frustrating defect bonds with finite concentration destroy the long-range order in the two-dimensional collinear magnets. Instead, the SRO order of the glassy phase emerges in the system [28, 29]. Strong defects lead to additional rotations of spins, $\delta\varphi(\mathbf{r})$, in the classical ground state of the system. For a single defect bond, they can be described as the dipolar field (cf. Refs. [27,30]),

$$\delta\varphi(\mathbf{r}) = \frac{\mathbf{d}\cdot\mathbf{r}}{r^D}, \tag{3}$$

where $\mathbf{d}$ is the dipole moment of the defect bond, $\mathbf{r}$ is the distance from the defect bond, and D is the dimension of the system. After averaging over disorder configurations, one gets for mean squared transverse fluctuation of the ordered moment M [31]:

$$\langle M_\perp^2\rangle \sim xM^2\int d^Dr\,\delta\varphi^2(\mathbf{r}). \tag{4}$$

In two-dimensional systems, this integral diverges as a logarithm on large distances and the cut-off (disorder-induced correlation length ξ_d) should be introduced. Importantly, ξ_d is finite for every nonzero concentration x. In three-dimensional systems, the same scenario can occur at finite concentrations x_c if the disorder is strong enough [29]. Correlation length can be estimated using the condition

$$1 = x\int^{\xi_d} d^3r\,\delta\varphi^2(\mathbf{r}), \tag{5}$$

which at $x > x_c$ yields

$$\xi_d \sim (x - x_c)^{-1}. \tag{6}$$

Note, that the correlation length ξ_d is temperature-independent since its nature is pure classical.

In the considered mixed B20 helimagnet, the LRO disappears at $x_c \approx 0.11$. The correlation length ξ_d decreases from infinity at x_c to finite values at larger Fe concentrations. We denote disorder-induced inverse correlation length as κ_d. When discussing polarized neutron scattering data, κ_d^2 should be added into the denominator of Eq. (1) and considered as a part of κ^2 along with temperature-dependent contribution κ_T^2 as the system has effective size ξ_d [32].

Thus, we arrive to the following qualitative picture. The sample with $x = 0.10$ has $\kappa_d = 0$ and behaves like pure MnSi with lower T_c and T_{DM} values due to AF bonds-induced lowering of the spin-wave stiffness. Half-moon patterns and sharp peaks in the neutron scattering (see Figs. 2 and 3), and peaks in magnetic susceptibility [22] near T_c are well pronounced due to mean-field denominator propotional to $(Q-k)^2 + \kappa_T^2$.

For the sample with $x = 0.15$, the inverse correlation lenght κ_d is nonzero and it is smaller than k. It leads to the highly chiral fluctuating phase at $T < T_{DM}$, but suppresses the growth of the critical fluctuations so naturally seen at $x < x_c$. Moreover, since κ has a tendency to saturation upon temperature lowering (see Fig. 4), apparently there should be a transition to frozen SRO phase (like in usual spin-glasses, see Ref. [33]) with correlation length larger than the spiral period. In the polarized neutron images, such behaviour results in blurred half-moon patterns, whereas in magnetic susceptibility measurements [22] there is a broad maximum.

At $x = x_{DM}$, spin wave stiffness becomes zero, and a possible qualitative description of the experimental data observed at $x > x_{DM}$ (e. g., blurred SANS maps and negative Curie–Weiss temperature) can be based on a domination of the AF interaction in the sample. Concentration x_{DM} itself is very peculiar, its vicinity in T–x phase diagram should reveal intriguing properties of the fluctuating highly chiral helical state with the shortest period possible for such systems. The correlation length of these fluctuations are affected by two factors not related to temperature: disorder induced by the AF bonds and DM interaction destabilizing the ferromagnetic order. A detailed description of the situation in the vicinity of x_{DM} requires further experimental studies.

Funding. The authors thank for the support the Russian Science Foundation (grant No. 17-12-01050).

The full text of this paper is published in the English version of JETP.

REFERENCES

1. L. Lundgren, O. Beckman, V. Attia, S. P. Bhattacherjee, and M. Richardson, Phys. Scripta **1**, 69 (1970).

2. Y. Ishikawa, K. Tajima, D. Bloch, and M. Roth, Sol. St. Comm. **19**, 525 (1976).

3. I. Dzyaloshinskii, J. Phys. Chem. Sol. **4**, 241 (1958).

4. T. Moriya, Phys. Rev. **120**, 91 (1960).

5. S. Muhlbauer, B. Binz, F. Jonietz, C. Pfleiderer, A. Rosch, A. Neubauer, R. Georgii, and P. Böni, Science **323**, 915 (2009).

6. O. Nakanishia, A. Yanase, A. Hasegawa, and M. Kataoka, Sol. St. Comm. **35**, 995 (1980).

7. P. Bak and M. H. Jensen, J. Phys. C **13**, L881 (1980).

8. S. V. Grigoriev, N. M. Potapova, S.-A. Siegfried, V. A. Dyadkin, E. V. Moskvin, V. Dmitriev, D. Menzel, C. D. Dewhurst, D. Chernyshov, R. A. Sadykov, L. N. Fomicheva, and A. V. Tsvyashchenko, Phys. Rev. Lett. **110**, 207201 (2013).

9. K. Shibata, X. Z. Yu, T. Hara, D. Morikawa, N. Kanazawa, K. Kimoto, S. Ishiwata, Y. Matsui, and Y. Tokura, Nature Nanotechnology **8**, 723 (2013).

10. S. V. Grigoriev, A. S. Sukhanov, and S. V. Maleyev, Phys. Rev. B **91**, 224429 (2015).

11. Y. Nishihara, S. Waki, and S. Ogawa, Phys. Rev. B **30**, 32 (1984).

12. S. V. Grigoriev, V. A. Dyadkin, E. V. Moskvin, D. Lamago, Th. Wolf, H. Eckerlebe, and S. V. Maleyev, Phys. Rev. B **79**, 144417 (2009).

13. S. V. Grigoriev, E. V. Moskvin, V. A. Dyadkin, D. Lamago, T. Wolf, H. Eckerlebe, and S. V. Maleyev, Phys. Rev. B **83**, 224411 (2011).

14. S. V. Demishev, I. I. Lobanova, V. V. Glushkov, T. V. Ischenko, N. E. Sluchanko, V. A. Dyadkin, N. M. Potapova, and S. V. Grigoriev, JETP Lett. **98**, 829 (2013).

15. A. Bauer, A. Neubauer, C. Franz, W. Munzer, M. Garst, and C. Pfleiderer, Phys. Rev. B **82**, 064404 (2010).

16. S. V. Demishev, V. V. Glushkov, S. V. Grigoriev, M. I. Gilmanov, I. I. Lobanova, A. N. Samarin, A. V. Semeno, and N. E. Sluchanko, Phys.-Uspekhi **59**, 559 (2016).

17. S. Tewari, D. Belitz, and T. R. Kirkpatrick, Phys. Rev. Lett. **96**, 047207 (2006).

18. F. Kruger, U. Karahasanovic, and A. G. Green, Phys. Rev. Lett. **108**, 067003 (2012).

19. V. V. Glushkov, I. I. Lobanova, V. Yu. Ivanov, V. V. Voronov, V. A. Dyadkin, N. M. Chubova, S. V. Grigoriev, and S. V. Demishev, Phys. Rev. Lett. **115**, 256601 (2015).

20. S. V. Grigoriev, S. V. Maleyev, E. V. Moskvin, V. A. Dyadkin, P. Fouquet, and H. Eckerlebe, Phys. Rev. B **81**, 144413 (2010).

21. M. Janoschek, M. Garst, A. Bauer, P. Krautscheid, R. Georgii, P. Böni, and C. Pfleiderer, Phys. Rev. B **87**, 134407 (2013).

22. L. J. Bannenberg, F. Weber, A. J. E. Lefering, T. Wolf, and C. Pappas, Phys. Rev. B **98**, 184430 (2018).

23. S. V. Grigoriev, E. V. Altynbaev, S.-A. Siegfried, K. A. Pschenichnyi, D. Menzel, A. Heinemann, and G. Chaboussant, Phys. Rev. B **97**, 024409 (2018).

24. *The data reduction software used is Graphical Reduction and Analysis SANS Program* (*GRASP*), www.ill.eu/instruments-support/instruments-groups/groups/lss/grasp/.

25. S. V. Grigoriev, S. V. Maleyev, A. I. Okorokov, Y. O. Chetverikov, R. Georgii, P. Böni, D. Lamago, H. Eckerlebe, and K. Pranzas, Phys. Rev. B **72**, 134420 (2005).

26. N. M. Chubova, E. V. Moskvin, V. A. Dyad'kin, Ch. Dewhurst, S. V. Maleev, and S. V. Grigor'ev, JETP **125**, 789 (2017).

27. O. I. Utesov, A. V. Sizanov, and A. V. Syromyatnikov, Phys. Rev. B **92**, 125110 (2015).

28. A. Aharony, R. J. Birgeneau, A. Coniglio, M. A. Kastner, and H. E. Stanley, Phys. Rev. Lett. **60**, 1330 (1988).

29. V. Cherepanov, I. Y. Korenblit, A. Aharony, and O. Entin-Wohlman, Eur. Phys. J. B **8**, 511 (1999).

30. I. Ya. Korenblit, Phys. Rev. B **51**, 12551 (1995).

31. S. Dey, E. C. Andrade, and M. Vojta, Phys. Rev. B **101**, 020411(R) (2020).

32. A. Z. Patashinskii and V. L. Pokrovskii, *Fluctuation Theory of Phase Transitions*, Pergamon Press (1979).

33. S. L. Ginzburg, *Irreversible Phenomena of Spin Glasses* (in Russian), Nauka, Moscow (1989).